Int. J. Heat Mass Transfer. Vol. 13, pp. 491–502. Pergamon Press 1970. Printed in Great Britain

NEUTRON RADIOGRAPHIC STUDY OF LIMITING PLANAR HEAT PIPE PERFORMANCE

RICHARD A. MOSS

Department of Mechanical Engineering, Massachusetts Institute of Technology, Cambridge, Massachusetts

and

ARNOLD J. KELLY

Guggenheim Laboratories, Princeton University, Princeton, New Jersey

(*Received* 3 *February* 1969 *and in revised form* 26 *August* 1969)

Abstract—A condition limiting the maximum heat transfer rate attainable by heat pipes has been investigated experimentally. Using neutron radiographic techniques, a detailed investigation of the vaporization processes which occur interior to the wick structure of a planar heat pipe employing water as a working fluid was conducted for a number of wicks having different mean pore sizes and for several angles of inclination of the wick.

The neutron radiographic system employed permitted measurements of the liquid layer thickness, in the wick, to be made with an accuracy of 0·006 in. for thicknesses up to 0·125 in. of water, and with a lateral resolution of 0·0135 in.

Two models of the heat transfer process occurring in planar heat pipes were postulated and analytically formulated. The first model assumed that evaporation occurred only from the upper surface of the wick whereas the second assumed that vapor was generated at the wick's base and released solely from the sides of the wick. With a secondary assumption of variable pore size, the second model proved to be more realistic for correlating the test date than the first.

The apparent variation of pore size, indicated by the data to be a function of heat transfer rate, has been interpreted as a manifestation of the "Leverett effect".

NOMENCLATURE

g, gravity [ft/h^2];
k, thermal conductivity [Btu/ft°F h];
K, permeability [ft^2];
L, length [ft];
P, pressure [lb/ft^2];
q, heat flux [Btu/ft^{2}h];
R, gas constant [Btu/lb°F];
r_p, pore radius [ft];
S, wick thickness [ft];
τ, vapor blanket thickness [ft];
T, temperature [°F];
v, velocity [ft/h];
W, width [ft];
θ, wick inclination angle;
φ, contact angle;
γ, surface tension [lb/ft];
λ, latent heat of vaporization [Btu/lb];
ρ, density [lb/ft^3];
μ, viscosity [lbh/ft^2].

Subscripts

cap, capillary;
e, evaporator;
g, vapor;
l, liquid;
0, saturation conditions;
t, transmission section.

INTRODUCTION

THE HEAT pipe [1–4] (see Fig. 1) is an engineering device for transporting heat at virtually isothermic conditions [1]. Heat is absorbed in the evaporator section and is manifested as the latent heat evaporization of the working fluid.

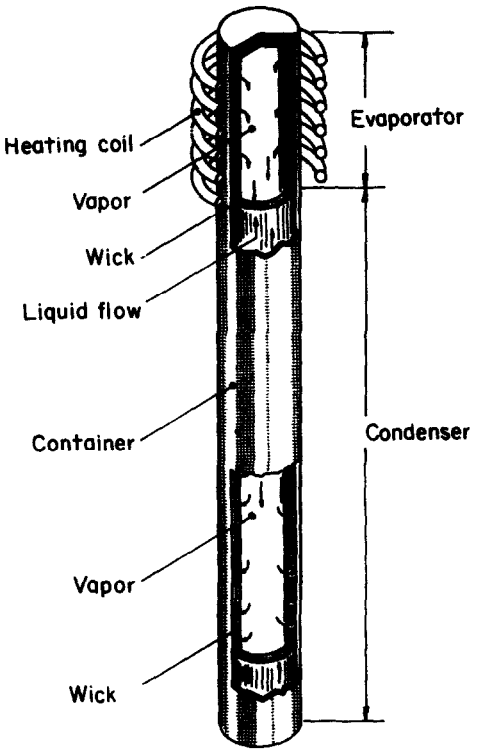

FIG. 1. The Grover heat pipe.

A lower vapor pressure exists in the condenser section, consequently the vapor flows to the condenser wherein it condenses and releases its latent heat of vaporization. The condensate liquid is absorbed by the wick and flows under the action of capillary forces back to the evaporator section where vaporization occurs and the cycle, which operates continuously, is complete. This transport of the latent heat of vaporization from the evaporator section to the condenser section constitutes the primary mechanism for energy transport.

The heat pipe, because of its unique mode of operation which makes it virtually insensitive to gravitational effects and its ability to transfer heat in an almost isothermic manner, is particularly amenable to operation in space, as well as to a wide variety of terrestial applications.

One of the least understood aspects of the operation of the heat pipe is the "boiling" process that occurs inside the wick at high heat transfer rates. Under conditions of high heat transfer rate, it is possible for the wick to dry out, an undesirable effect, which could lead to a temperature excursion in, and possible destruction of, the evaporator section. Drying of the wick under high heat transfer rate conditions can be conceived as occurring in two fundamentally different ways. The first stems from the fact that heat transfer to the heat pipe results in the internal refluxing of working fluid in the device. The greater the heat transfer rate, the higher the refluxing rate of the fluid. At some critical heat transfer rate, the capillary pressure differential in the wick will be insufficient to drive the liquid through the heat pipe; causing the wick to dry in the vicinity of the evaporator section. The wick can also dry out from the effects of the formation of vapor at the base of the evaporator section due to heating. Such vapor could act to form either a partial or complete vapor lock in the wick and thereby prevent additional liquid from being drawn into the evaporator.

An experimental investigation of the manner in which vapor actually forms in the wick of a planar heat pipe, as a function of heat transfer rate and the physical characteristics of the wick, form the basis of this research.

EXPERIMENT

Water was selected as the most desirable heat transfer fluid for this investigation since it possessed the substantial advantages of having (1) well-known properties, (2) relatively low boiling point, (3) convenient working fluid characteristics, e.g. it is nonflammable, inexpensive,

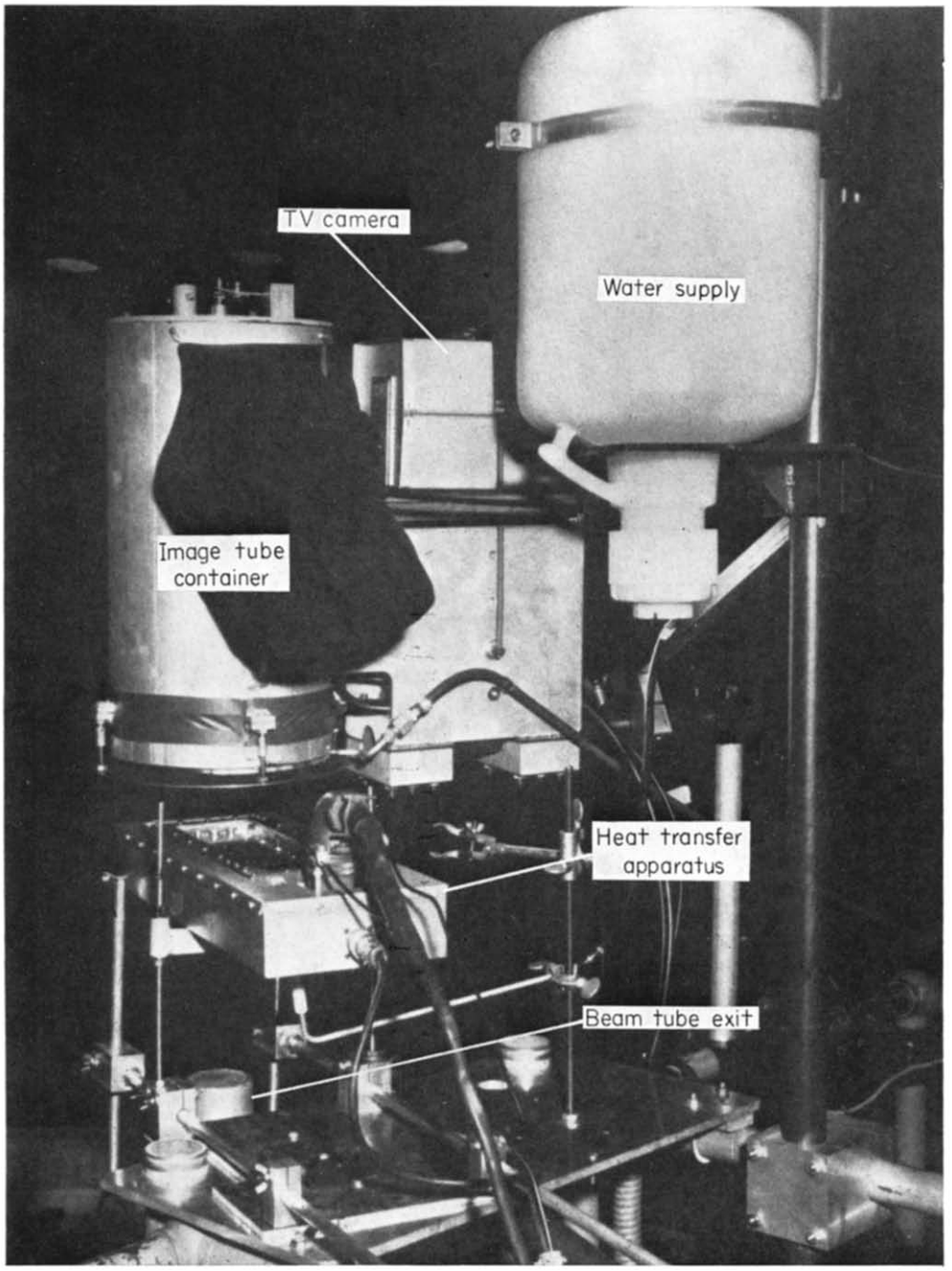

FIG. 2. Photograph of test apparatus.

[*facing page* 492]

non-corrosive, and non-toxic, and (4) is available at high purity levels.

Since water is hydrogenous, it became evident that neutron radiography could best provide information on the phenomenological behavior of water inside the wick during the heat transfer process. Furthermore, this diagnostic technique does not influence the phenomena being studied as it can be demonstrated that nucleation of the superheated water in the wick caused by the absorption of radiation associated with the neutron radiographic measurement is negligible under the conditions prevailing in the experiment.

A photograph of the test apparatus is shown in Fig. 2. The neutron source for these experiments was derived from the Industrial Reactor Laboratory (located in Plainsboro, New Jersey) 5 MW swimming pool reactor. The neutron beam was obtained by vertically positioning a hollow, air filled aluminium tube in juxtaposition with the nuclear reactor core which was submerged at the bottom of the water pool. The "beam tube" (~30 ft long and 3 in. dia.) together with the experimental apparatus was mounted on a movable carriage. A collimated neutron beam was emitted from the tube with a neutron intensity of approximately 10^7 thermal neutrons/cm^{2}s when the tube was brought close to the face of the reactor core.

The heat transfer apparatus was positioned such that the neutron beam emanating from the collimating tube passed through the evaporator section of the planar heat pipe. The local neutron beam was, therefore, reduced according to the amount of water penetrated and an image was thus impressed on the neutron beam in exactly the same way that an image is impressed on a X-ray beam after passage through an absorbing or scattering media. Like X-ray radiography, neutron radiography is capable of yielding information only on the total thickness of material penetrated. The beam, attenuated by the presence of the water in the wick, passes into the imaging system and finally into a "beam-catcher" where it is absorbed and dissipated to an acceptable level, consistent with safety requirements.

The imaging system used a thermal neutron image intensifier tube, specifically designed to electronically convert the thermal neutron "image" into an amplified visible image [5]. This image was either monitored remotely with a T.V. system or photographed directly with a still camera. The water content of the wick in the area traversed by the neutron beam was determined by processing the camera photonegatives in a recording microphotodensitometer and comparing the intensity measurements with those from calibrated water depths. Using this technique, it was possible to reproducibly measure water thicknesses to $\pm 0{\cdot}006$ in. with an experimentally determined lateral resolution of 0·0135 in.

The three different planar wicks tested were constructed of layers of stainless steel wire mesh sintered to form a continuous isotropic structure. A sintered mesh construction was chosen since it would insure that the wick structure would remain invariant during the testing program and would provide a highly uniform isotropic structure, i.e. uniform porosity. Planar rather than cylindrical wick geometry was chosen to eliminate the ambiguities associated with the interpretation of the image formed when the neutron beam interacted with the two sides of a cylindrical wick.

The three different wicks which were tested possessed the following physical characteristics:

Mesh size	Screen layers	Wick thickness, S, (in)	Mean pore radius r_p (ft)
100	38	0·250	$2{\cdot}3 \times 10^{-4}$
150	60	0·250	$1{\cdot}7 \times 10^{-4}$
200	72	0·240	$1{\cdot}2 \times 10^{-4}$

These wicks, 10 in. long and 2 in. wide had a void fraction of approximately $\frac{1}{2}$. Consequently the $\frac{1}{4}$ in. wicks contained about $\frac{1}{8}$ in. thickness of water, the exact amount, of course, being determined by the neutron diagnostic technique.

A wick undergoing test was mounted in the heat transfer apparatus shown in Fig. 2. This apparatus was designed specifically to offer minimal attenuation of the neutron diagnostic beam. The section of the wick studied, i.e. the 2 in. long evaporator section, was heated by an electric strip heater which not only provided uniform heating of this section of the wick but presented minimum interaction with the operation of the neutron image tube. Teflon coated copper–constantan thermocouples, referenced to boiling water, were used to monitor the temperature in the evaporator and transmission sections of the wick and in the container proper. These thermocouples were monitored continuously during a test to provide, (1) assurance that the heat pipe was operating correctly, and (2) to provide information as to when steady state conditions had been attained after the heat input had been changed to a new level. The container, sealed so as to prevent the escape of water vapor and operated at atmospheric pressure, was heated slightly to prevent condensation of water vapor on the container walls in the vicinity of the evaporator section. Since the neutron radiographic probe yields information on the total integrated water thickness penetrated and not its distribution in a direction parallel to the neutron flight path, condensate on the container walls, if present, would yield spurious results for the water thickness in the wick.

Triply distilled and chemically pure water (0·1 ppm impurities) was employed in all tests. Prior to the start of each test series, the wick to be tested was boiled for several hours in water. This ensured that the wick would be completely saturated and free of any voids or air spaces. The water was metered as it was introduced into the condensate end of the wick. The stream evolved during test was ducted away from the container and condensed externally. This measurement of the water flux rate provided an independent check on the heat flux supply to the evaporator. It should be mentioned that limitations on the heater design prevented operation of the wicks studied at heat flux levels in excess of 40000 Btu/hft^2.

The heat transfer apparatus and neutron imaging system were designed so as to permit operation at wick inclination angles (θ) of up to 20° with respect to horizontal. Data were collected at inclination angles of 10° and 20° as shown in Figs. 4–9.

ANALYTICAL

The objective of the analysis was to quantitatively predict the vapor blanket size as a function of heat transfer rate. All fluid properties, with the exception of vapor pressure, were considered to be constant.

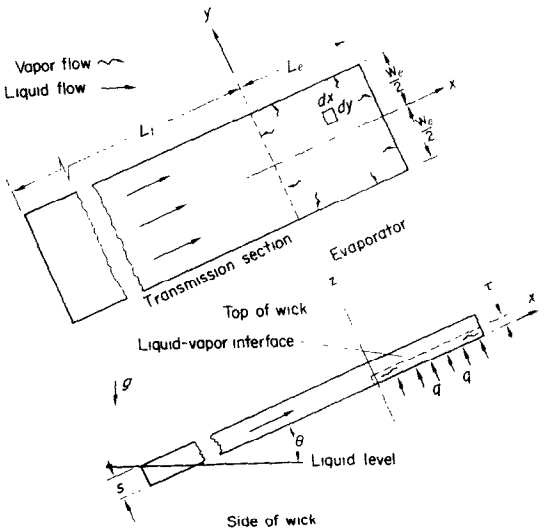

FIG. 3. Systems of coordinates—planar heat pipe.

The system being examined is shown in Fig. 3. Water is absorbed by the wick at position $x = -L_t$ and is drawn by capillary action through the transmission section into the evaporator. Vapor is generated when heat transfer to the wick causes evaporation of the working fluid. Two fundamentally different heat-mass transfer mechanisms have been postulated to occur in the evaporator section of the wick. In one model it was assumed that heat is transferred by conduction to the upper surface

of the wick where evaporation thereupon occurs. A static (time invariant) vapor blanket is presumed to exist at the base of the wick; and the position of the liquid–vapor interface is fixed by the balance between the vapor pressure and the capillary pressure. In the other model, it was postulated that heat would be transferred by conduction to an internal liquid–vapor interface where vapor is generated. This vapor, forming a blanket at the wick's base, was assumed to be released solely from the sides of the wick.

Darcy's Law, i.e.

$$v = \frac{K}{\mu}\left(\frac{dP}{dx} + \rho \sin\theta\right), \tag{1}$$

was assumed valid for describing the flow in the porous media of the wick. The pressure of the liquid in the evaporator section was calculated using Darcy's Law and by assuming that all heat delivered to the evaporator was manifested in the form of latent heat of vaporization. On this basis, one can show:

$$\Delta P_t = -\left[\frac{qL_e\mu_l}{\lambda\rho_l SK} + \rho_l \sin\theta\right]L_t. \tag{2}$$

The capillary pressure differential at the liquid–vapor interface is predicted by Young's equation,

$$\Delta P_{cap} = \frac{2\gamma\cos\varphi}{r_p}, \tag{3}$$

where r_p is the mean pore size of the wick.

In the first model, heat is conducted through the vapor blanket to the surface of the wick. The heat flow through the vapor blanket can be expressed as:

$$q = k\frac{T_{li} - T_0}{S - \tau}. \tag{4}$$

The liquid in the wick must be in equilibrium with the vapor in the vapor blanket. However, the heat transfer conditions of the model require that the liquid temperature at the liquid–vapor interface to be higher than the saturation temperature. This, in turn, requires an increase in vapor pressure of the liquid. For equilibrium, this increase in vapor pressure must be balanced by the capillary pressure at the liquid–vapor interface. The Clausius–Clapeyron equation,

$$\Delta P_g = \frac{P_0\lambda}{RT_0^2}\Delta T, \tag{5}$$

was used to relate the change in vapor pressure to the superheat temperature.

The pressure equation for equilibrium at the internal liquid–vapor interface is:

$$P_g - P_0 = \Delta P_t + \Delta P_{cap}. \tag{6}$$

Substituting equations (2), (3), (5) and (6) into equation (4) and solving for τ, one obtains:

$$\tau = S - \frac{kRT_0^2}{qP_0\lambda}\left[\frac{2\gamma\cos\varphi}{r_p} - \rho_l L_t \sin\theta - \frac{qL_eL_t\mu_l}{\lambda\rho_l KS}\right]. \tag{7}$$

Equation (7) is valid only when the predicted τ is greater than zero and less than S. A negative τ indicates that the capillary pressure has collapsed the vapor blanket: greater than S indicates the wick is dried out.

Now let us consider the second model. The liquid pressure in the evaporator is given by equation (2). Assuming a constant vapor blanket thickness (as in Model 1) and a spatially isotropic permeability and performing a mass balance across a differential element of area of the evaporator, it can be shown that:

$$\frac{\partial^2 P_g}{\partial x^2} + \frac{\partial^2 P_g}{\partial y^2} = -\frac{q\dot{\mu}_g}{\tau\lambda\rho_g K}. \tag{8}$$

In the experiments, steam could escape from the boundaries at $x = 0$, L_e and $y = \pm (W_e/2)$.

By translating P_g such that P_0 is zero, it is seen that the proper boundary condition is: $P_g = 0$ at the boundaries of the wick.

The solution to equation 8 incorporating the boundary conditions is:

$$\Delta P_g(x,y) = \frac{16L_e^2 q\mu_g}{\tau\pi^4\lambda\rho_g K}\sum_{n=1}^{\infty}\sum_{m=1}^{\infty}\frac{\cos\left[(2n-1)\frac{\pi x}{L_e}\right]\cos\left[(2m-1)\frac{\pi y}{W_e}\right](-1)^{m+n}}{\left[(2n-1)^2\left(\frac{L_e}{W_e}\right)^2+(2m-1)^2\right](2n-1)(2m-1)} \tag{9}$$

The pressure differential between the steam in the vapor blanket and the liquid can nowhere exceed the maximum pressure differential that can be sustained by the capillary forces in the wick. More precisely,

$$\Delta P_{cap} \geqslant \Delta P_g + \Delta P_l. \tag{10}$$

Since the pressure changes in the liquid over the length of the evaporator are small, the position of the maximum pressure differential between the liquid and vapor is determined by the gas flow in the vapor blanket. From Fig. 3 it is seen that the maximum pressure differential occurs at the origin. The vapor blanket thickness τ, at the origin ($x = y = 0$) for the wicks employed in the experiment ($L_e/W_e = 1$), is, from equations (2), (9) and (10):

$$\tau = 0{\cdot}0722\frac{L_e^2 q\mu_g}{\lambda\rho_g K\left[\frac{2\gamma\cos\varphi}{\lambda\rho_g K} - \rho_l q L_t \sin\theta - \frac{qL_e L_t\mu_l}{\lambda\rho_l K s}\right]}. \tag{11}$$

DISCUSSION

The analytical predictions of τ as a function of heat transfer rate for the two models are presented in Figs. 4–9 along with the experiheat transfer rate for the two models are presented in Figs. 4–9 along with the experimentally measured values of this parameter.

The liquid contact angle, φ (the angle formed between a solid and a liquid at the contact point) is a very important parameter in analyzing these results. Only limited data on contact angle are available and, furthermore, these data are not very reproducible. The question then immediately arises as to what is the actual value of the contact angle in these experiments.

On comparison with the experimental results shown in Figs. 4–9, it is seen there exists *no value* of contact angle which would permit a theoretical curve based on the first model to correlate the data at any heat transfer rate. There are, however, values of contact angle for which the theoretical curves based on the second model do lie in the same range as the data. For this reason, it is concluded that although both models of heat transfer (Models 1 and 2) probably occur simultaneously, the second model must be considered the most realistic. In these experiments, different wick cleaning techniques yielded different results which can most reasonably be explained in terms of a change in the contact angle (see Fig. 6).

As seen from Figs. 4–9, the data taken at the higher heat transfer rates diverges from the analytically predicted trend. The most probable explanation of this behavior is that the capillary pressure differential across the internal liquid–

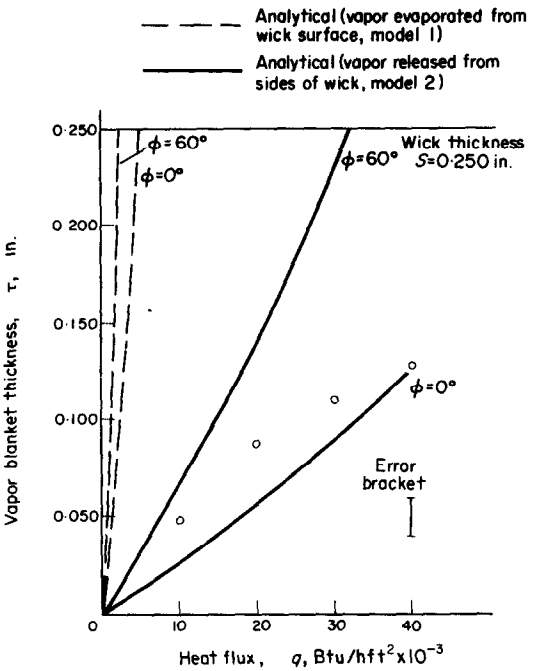

FIG. 4. Vapor blanket thickness as a function of heat transfer rate 100 mesh—10° inclination.

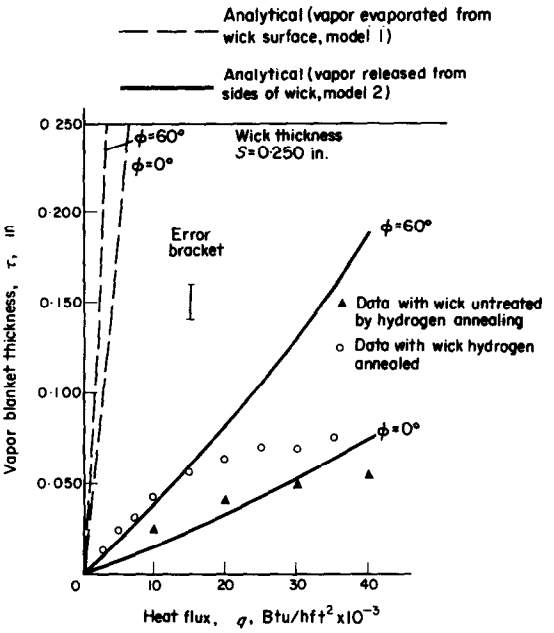

FIG. 6. Vapor blanket thickness as a function of heat transfer rate 150 mesh—10° inclination.

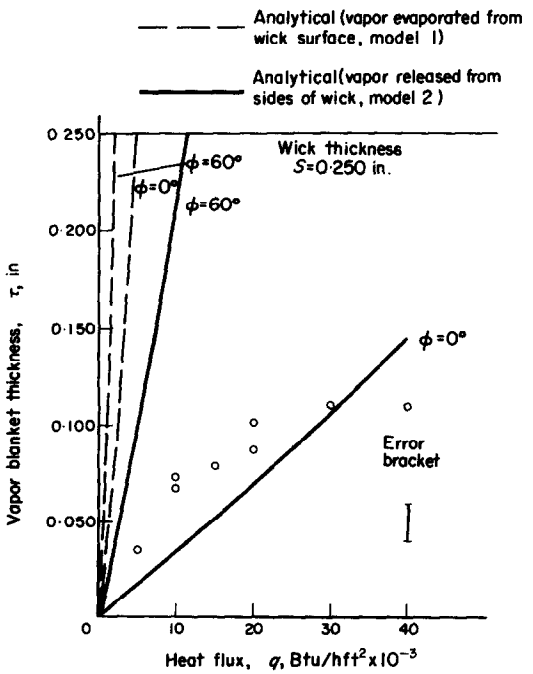

FIG. 5. Vapor blanket thickness as a function of heat transfer rate 100 mesh—20° inclination.

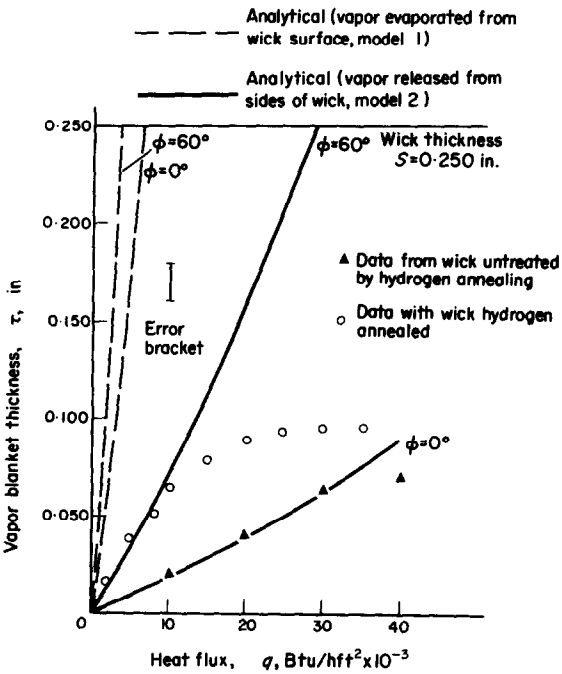

FIG. 7. Vapor blanket thickness as a function of heat transfer rate 150 mesh—20° inclination.

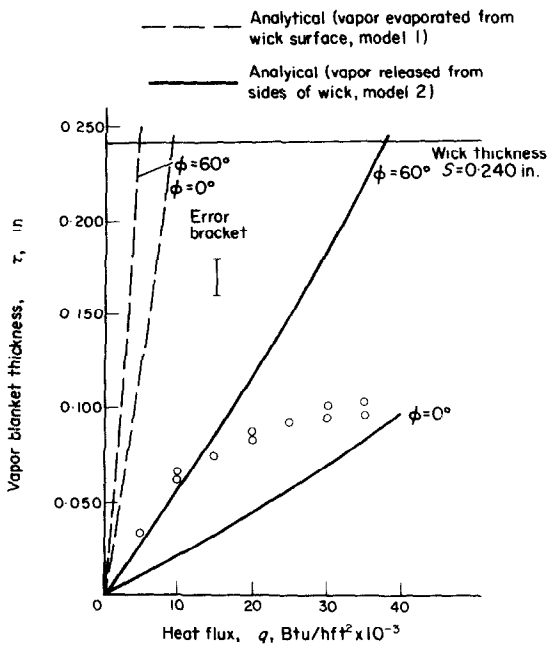

FIG. 8. Vapor blanket thickness as a function of heat transfer rate 200 mesh—10° inclination.

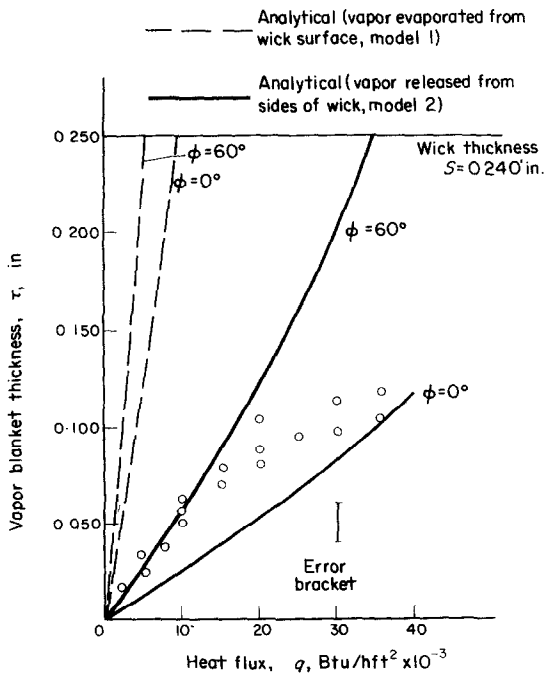

FIG. 9. Vapor blanket thickness as a function of heat transfer rate 200 mesh—20° inclination.

vapor interface is not constant, but rather increases with increasing heat transfer.

The justification for this proposition has its basis in the "Leverett effect" [6]. Capillary pressures far in excess of those expected on the basis of the mean pore size of the wick can be generated when the saturation (per cent of the void space filled with water) is less than 100 per cent. Normally any heating reduces the water saturation to zero (drives out any residual water) and the effect completely disappears. However, it is quite possible that, because of the nature of the heat transfer mechanism of Model 2, the boiling at the liquid–vapor interface in the wick becomes sufficiently intense so that liquid is

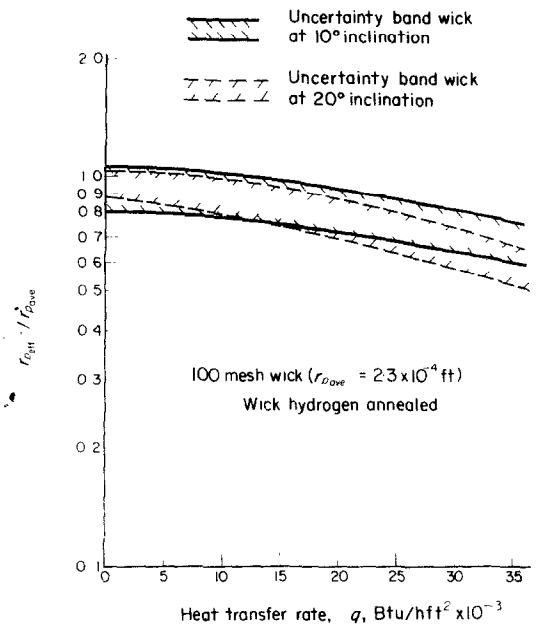

FIG. 10. Capillary pore size as a function of heat transfer rate.

replenished in a small portion of the vapor blanket as soon as it is evaporated. Under these circumstances, the capillary pressure differential would be greater than one would predict on the basis of mean pore size alone.

Figures 10–13 present the variations in effective pore radius r_{peff} (where $r_{peff} \leqslant r_{pave}$) as a function of heat transfer rate, necessary to

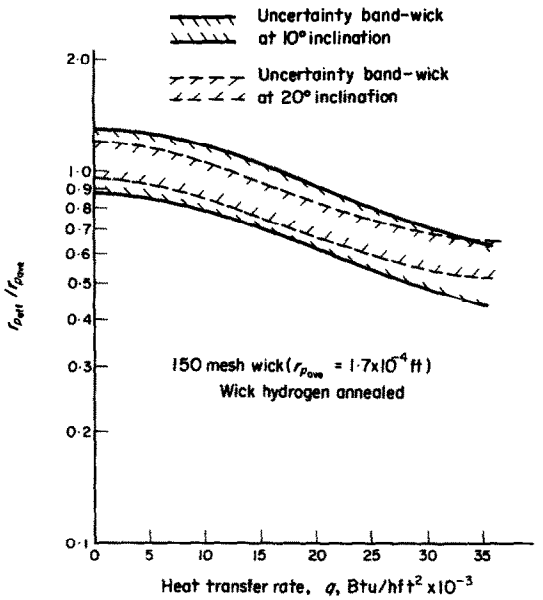

FIG. 11. Capillary pore size as a function of heat transfer rate.

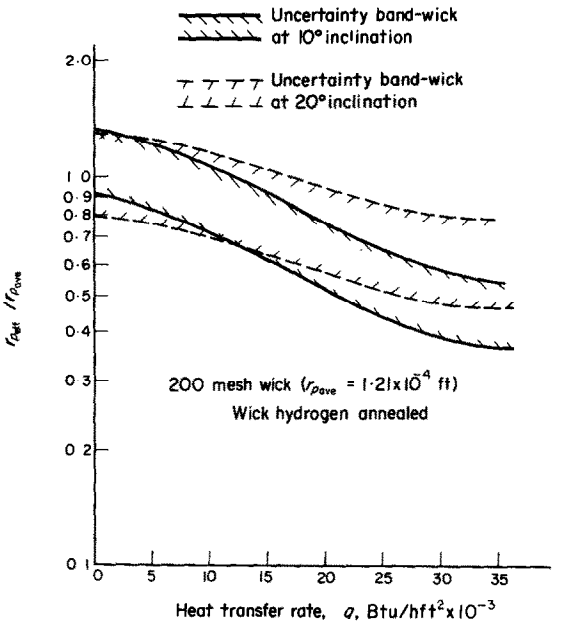

FIG. 13. Capillary pore size as a function of heat transfer rate.

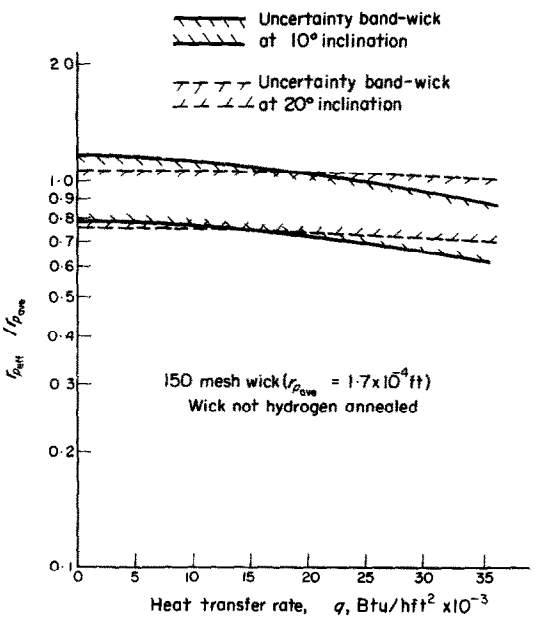

FIG. 12. Capillary pore size as a function of heat transfer rate.

reconcile the data of Figs. 4–9 with theory (Model 2), assuming that the contact angle is constant, i.e. independent of heat transfer rate. In general only a modest variation of the effective pore radius as a function of heat transfer rate (i.e. $1 \geqslant r_{peff}/r_{pave} \geqslant \frac{1}{2}$) is required to provide agreement between theory (Model 2) and experiment thereby lending credence to the supposition that the "Leverett effect" is influencing the behavior of the wick.

Neutron radiographic examination of the boiling process in the wick via a television monitor was used to determine if transient phenomena were taking place. Conclusions, however, are stated in semi-quantitative terms since there were no means available, other than unaided visual estimates, to quantify the magnitude of the transient effects. Furthermore, an image shimmering effect arising from the low neutron fluxes employed, further increased the difficulties associated with an evaluation of transient effects. Nevertheless, it was felt possible to detect, by observation, thickness changes in

$\frac{1}{8}$ in. of water amounting to approximately 10–20 per cent. Within these limits no large scale transient phenomena (of the magnitude observed in pool boiling) were observed.

It should be mentioned, however, that numerous small vapor patches could be seen in the wick oscillating (not in phase), in thickness, at approximately $\frac{1}{3}$ cps. Typically these vapor patches were approximately $\frac{1}{2}$ in. dia. From these observations, it would appear better to characterize these oscillations as waves on a surface rather than as individual bubbles as occurs in nucleate pool boiling. It is concluded that the presence of a porous structure in a boiling fluid has the effect of smoothing out the formation of individual nucleate bubbles and eliminates the sudden transition from nucleate to film boiling that is observed in pool boiling.

In applying the results of this work to heat pipes, one might reasonably ask how steam evolved at the base of the wick structure in a heat pipe could escape. It must be emphasized that the volume flow of gas, even for large heat transfer rates, is not, in general, very large and even small openings could suffice to release the steam. One could speculate that the steam would escape through the space between the front of the wick and the end of the heat pipe. In addition, wicks in heat pipes are generally constructed of rolled-up screens which would not provide an intimate and uniform contact between the wick and the heat pipe wall. In this case, the gaps between the wick and the wall would provide additional vapor passages. Under these circumstances, one would not expect a uniform vapor blanket to occur and hot spots would develop in the regions of greatest thermal resistance.

SUMMARY

The results of this work may be summarized as follows:

1. In describing boiling within a wick structure, a heat transfer model based on vapor escaping from the sides of the wick is more realistic than the model based on evaporation from the surface.
2. The capillary pressure differential inside a porous structure undergoing heat transfer is not constant, but rather is a function of heat transfer rate. This behavior can be qualitatively explained on the basis of the "Leverett effect."
3. Contact angle (φ) is an important parameter in considering wick boiling characteristics.
4. The presence of vapor in a wick will not automatically lead to a "vapor-lock" condition.
5. While some transient effects were visible, they were much smaller in magnitude than what would be present in conventional pool boiling. In wick boiling, the frequency of transient phenomena ($\frac{1}{3}$ cps.) was much lower than has been observed in pool boiling.
6. In applying the results of the work to heat pipe systems, care must be taken that the assumptions used in this study are not violated. The principle assumptions are listed below:
   1. The vapor blanket thickness is smaller than a characteristic dimension of the wick's evaporator section.
   2. Constant wick thickness.
   3. Steady and constant heat input.
   4. Narrow pore size distribution.

ACKNOWLEDGEMENTS

The author gratefully acknowledges the contributions of the Industrial Reactor Laboratories, the Rauland Corporation, and the Greyrad Corporation to this research program.

REFERENCES

1. G. M. Grover, T. P. Cotter and G. F. Erickson, Structures of very high thermal conductance, *J. Appl. Phys.* **35**, 1990–1991 (1964).
2. J. Bohdansky, C. A. Busse and G. M. Grover, The use of new heat removal system in space thermionic power supplies, *EUR* 2229.3, European Atomic Energy Community (1965).
3. S. Katzoff, Heat pipes and vapor chambers for thermal control of spacecraft, *AIAA Thermophysics Specialist Conference* paper No. 67-310, April 17–20 (1967).
4. J. E. Deverall, J. E. Kemme, Satellite heat pipe, LA-3278-Ms, Los Alamos Sci. Lab., April 20 (1965).

5. H. BERGER, W. F. NIKLAS and A. SCHMIDT, An operational thermal neutron image intensifier, *J. Appl. Phys.* **36**, 2093–2094 (1965).

6. A. E. SCHEIDEGGER, *The Physics of Flow Through Porous Media*. Macmillan (1960).

ETUDE PAR LA RADIOGRAPHIE NEUTRONIQUE DES LIMITES DES PERFORMANCES D'UN CALODUC PLAN

Résumé—Une condition limitant le maximum du flux de chaleur qu'on peut atteindre avec des caloducs a été étudiée expérimentalement. On a conduit, en employant les techniques de la radiographie neutronique, une étude détaillée des processus de vaporisation qui se produisent à l'intérieur de la structure de la meche d'un caloduc plan utilisant de l'eau comme fluide moteur avec un certain nombre de mèches ayant différentes tailles moyennes de pores et avec plusieurs angles d'inclinaison de la mèche.

Le système de radiographie neutronique employé permettait des mesures de l'épaisseur de la couche liquide dans la mèche avec une précision de 150 μm pour une épaisseur allant jusqu'à 3,2 mm d'eau et avec une résolution latérale de 3,4 mm.

Deux modèles du processus de transport de chaleur dans les caloducs plans ont été admis et formulés analytiquement. Le premier modèle supposait que l'évaporation se produisait seulement à partir des surfaces supérieures de la mèche tandis que le second supposait que la vapeur était produite à la base de la mèche et libérée seulement à partir des côtés. Le second modèle, avec une hypothèse secondaire d'une taille variable des pores, a montré être plus réaliste que le premier pour corréler les résultats des essais.

La variation apparente de la taille des pores, que les résultats montrent être une fonction du flux de chaleur, a été interprétée comme étant une manifestation de l'"effet Leverett".

NEUTRONENRADIOGRAFISCHE UNTERSUCHUNG DER ARBEITSGRENZEN EBENER WÄRMEROHRE.

Zusammenfassung—Eine Bedingung welche den maximal erreichbaren Wärmetransport in Wärmerohren begrenzt, wurde experimentell untersucht. Unter Benützung der Neutronenradiografie wurde eine detaillierte Untersuchung der Verdampfungsprozesse durchgeführt wie sie im Innern von Dochtstrukturen ebener, wassergefüllter Wärmerohre auftreten. Es wurden eine Reihe von Dochten mit unterschiedlichen Porengrössen und verschiedene Neigungswinkel des Dochtes betrachtet.

Das benützte neutronenradiografische System gestattet Messungen der Schichtdicke der Flüssigkeit im Docht mit einer Genauigkeit von 0·15 mm für Schichtdicken von 3·17 mm und bei einer seitlichen Auflösung von 0·34 mm.

Für den in ebenen Wärmerohren auftretenden Wärmetransportprozess wurden zwei Modelle angenommen und analytisch formuliert. Nach dem ersten Modell erfolgt die Verdampfung nur an der oberen Fläche des Dochtes† entstehen soll und allein von den Dochtseiten abströmt. Mit einer Sekundärannahme für veränderliche Porengrösse erwies sich das zweite Modell für die Korrelation realistischer als das erste.

Die offensichtliche Veränderlichkeit der Porengrösse, die sich nach den Ergebnissen als eine Funktion des Wärmetransportes erweist, wurde als eine Bestätigung des "Leverett Effekts" angesehen.

† Während im zweiten Modell der Dampf nur an der Basis des Dochtes.

НЕЙТРОННОЕ РАДИОГРАФИЧЕСКОЕ ИССЛЕДОВАНИЕ ХАРАКТЕРИСТИК ПЛОСКИХ ТРУБЧАТЫХ ТЕПЛООБМЕННИКОВ

Аннотация—Проводилось экспериментальное изучение условия, ограничивающего максимальную скорость переноса тепла, достигаемую в трубчатом теплообменнике. С помощью нейтронной радиографии проведено детальное изучение процессов испарения, происходящих внутри структуры фитиля плоского теплообменника, в котором в качестве рабочей жидкости используется вода. Исследовался ряд фителей с различным средним размером пор и различными углами наклона фитилей.

Использованная нейтронная радиографическая система позволяла производить измерения толщины слоя жидкости в фитиле с точностью до 0,006 дюйма при толщине слоя воды в 0,125 дюйма и с горизонтальной разрешающей способностью в 0,0135 дюйма.

Постулировались и аналитически формулировались две модели процесса переноса тепла, происходящего в плоских трубчатых теплообменниках. Предполагалось, что в первой модели испарение происходит только с верхней поверхности фитиля, в то время как во второй модели иарообразование происходит у основания фитиля, и пар выделяется только с его боковых сторон. При вспомогательном допущении о переменном размере пор вторая модель по сравнению с первой оказалась более реальной для корреляции опытных данных.

Видимое изменение размеров пор, являющееся функцией скорости переноса тепла, объясняется как проявление эффекта Леверетта.